JOURNAL OF GEOPHYSICAL RESEARCH, VOL. 102, NO. B2, PAGES 3097–3108, FEBRUARY 10, 1997

Deepening of the axial magma chamber on the southern East Pacific Rise toward the Garrett Fracture Zone

Maya Tolstoy,[1] Alistair J. Harding, and John A. Orcutt

Institute of Geophysics and Planetary Physics, Scripps Institution of Oceanography, La Jolla, California

TERA Group[2]

Abstract. A wide-aperture profile along the ridge axis from 14°29′S to 13°39′S, 120 km to 30 km south of the Garrett Fracture Zone, is analyzed to constrain the thickness of layer 2a and the depth to the axial magma chamber reflector. Five areas along the 90 km line are examined in detail, with several consecutive gathers being analyzed for each area to establish the degree of consistency within each area. A genetic algorithm code is used to find a best fit model from a comparison of the data and WKBJ synthetic seismograms. One hundred starting models are generated using a predefined set of velocity nodes, with a fixed window of allowable depth variations between nodes. An evolutionary process favors the better fitting models in each generation, and a satisfactory misfit is usually obtained within 40 generations. Within individual areas the models were in good agreement with the depth of a given velocity node, generally varying by not more than 20 m, the depth discretization interval for the models. A consistent deepening trend of the axial magma chamber (AMC) is observed across the five areas as the Garrett Fracture Zone is approached. The depth varies from 0.99 km at area 1, which is approximately 100 km south of the Garrett, to 1.23 km at area 5, which is approximately 40 km south of the Garrett. The depth to the axial magma chamber is highly sensitive to any ship wander off axis since layer 2a thickens rapidly off axis with age. For the areas examined here, layer 2a is observed to be relatively constant in thickness along the axis, although it is about 40 m thicker over area 5, where the axial magma chamber is deepest. This variation is within the scatter of previously detailed layer 2a measurements at 13°N on the East Pacific Rise, where an effectively constant thickness is observed. This implies that layer 2a thickening is not a significant factor along this profile and that the AMC deepening is real rather than apparent. Theoretical modeling suggests that the depth to the lid of the axial magma chamber is related to the rate of heat supply at a given location. Thus the gradual consistent deepening of the axial magma chamber can be taken as an indication of a slightly reduced magma supply toward the Garrett Fracture Zone, which marks a major interruption of hundreds of kilometers of continuous ridge axis. The deepening may also be interpreted as a downward limb from a central injection point; however, there is no indication of a similar downward trend in the other (southern) direction. Furthermore, there is no accompanying systematic variation in axial depth or axial volume, both of which are proposed to be indicators of central injection and along-axis flow.

Introduction

The structure of the upper oceanic crust and depth to the axial magma chamber (AMC) can tell us much about the processes controlling the formation of crust. The evolution of layer 2a thickness provides insights into the emplacement mechanisms forming the upper crust, and the depth to the AMC may provide information regarding magma properties. The along-axis continuity of the magma chamber yields information on the segmentation of the spreading center, the dimensionality of the upwelling in the underlying mantle, and the likelihood of the mixing of magma along axis.

Upper crustal structure at slow spreading ridges is still not well understood but is thought to be fairly complex [*Purdy*, 1987]. In contrast, the upper crustal structure at fast spreading ridges has been analyzed in increasing detail in recent years, from the initial observation that layer 2a thickens with age [*McClain et al.*, 1985; *Toomey et al.*, 1990; *Christeson et al.*, 1992; *Harding et al.*, 1993a] to the detailed mapping of the variations in the style of thickening [*Kent et al.*, 1994]. The thickening of layer 2a with age has been confirmed by recent seismic work on the East Pacific Rise (EPR) [*Harding et al.*, 1989, 1993; *Vera et al.*, 1990; *Toomey et al.*, 1990; *Christeson et al.*, 1992, 1994; *Caress et al.*, 1992; *Kent et al.*, 1994]. Layer 2a at fast spreading ridges is often interpreted as extruded pillow basalts, while layer 2b is interpreted to be the intruded sheeted dike complex [*Harding et al.*, 1993a]. Detailed along-axis anal-

[1]Now at Lamont-Doherty Earth Observatory of Columbia University, Palisades, New York.

[2]Robert S. Detrick and Graham M. Kent, Department of Geology and Geophysics, Woods Hole Oceanographic Institution, Woods Hole, Massachusetts; John C. Mutter and Peter Buhl, Lamont-Doherty Earth Observatory of Columbia University, Palisades, New York.

Paper number 96JB03226.
0148-0227/97/96JB-03226$09.00

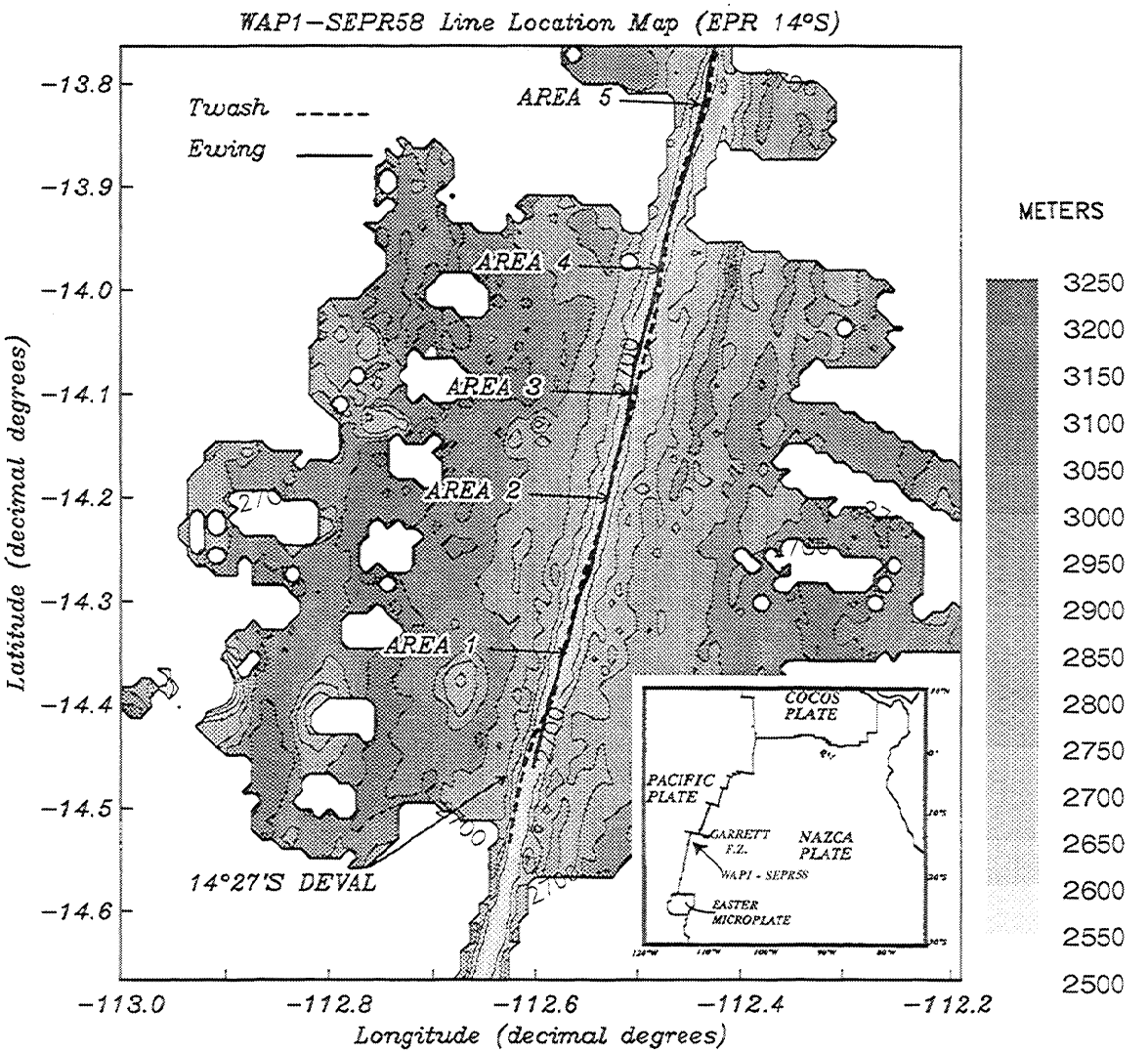

Figure 1. Bathymetric map of the southern East Pacific Rise 14°S area, with inset map showing the general location of area and the Garrett Fracture Zone. The solid line indicates the track of the R/V *Maurice Ewing*, and the dashed line indicates the track of the R/V *Thomas Washington*. The areas examined in detail are marked at the 0 km point of the gather, with the 7.4 km length of the gather following to the south. Note that just to the south of area 4 the *Washington* wanders slightly off track.

yses of layer 2a thickness at 13°N [*Kappus et al.*, 1995] have found a remarkable similarity in structure over ~60 km, suggesting that the on-axis thickness of layer 2a is controlled by the dynamics of emplacement rather than the overall level of the magma supply.

The 14°S area of the EPR is known to have a relatively shallow and fairly continuous magma chamber reflection with a constant along-axis layer 2a thickness [*Detrick et al.*, 1993a]. However, the style of off-axis thickening of layer 2a is seen to vary toward the 14°27'S discontinuity [*Kent et al.*, 1994].

The depth to the AMC is directly correlated with spreading rate [*Purdy et al.*, 1992; *Phipps Morgan and Chen*, 1993]. The AMC is thought to be located at the thermal freezing boundary [*Phipps Morgan and Chen*, 1993; *Hooft and Detrick*, 1993], and since faster spreading ridges are hotter, that freezing boundary will be shallower than on slower spreading ridges. Variations in AMC depth along axis could therefore be interpreted as variations in the axial-thermal structure, which is controlled by an equilibrium between heat supply and dissipation through hydrothermal and conductive cooling.

While upwelling and accretion at slow spreading ridges are considered to be highly focused and three-dimensional, the dimensionality of accretion processes at fast spreading ridges is not as clearly defined. The striking uniformity in crustal structure at fast spreading ridges suggests a predominantly two-dimensional process, yet detailed examination reveals three-dimensional elements. *Macdonald et al.* [1988] propose that variations in axial depth and cross-sectional area are caused by central points of melt injection (at the topographic highs), with along-axis flow of melt down the limbs of the axis, resulting in a relative deepening of the axis as the migrating magma loses hydraulic head. They further propose that this mechanism leads to a variety of scales of ridge segment discontinuities. A corollary of these hypotheses is that ridge segment discontinuities should be associated with a disappearance or decrease, in the width of the AMC. However, *Kent et al.* [1993a] have

shown that for the 9°N segment of the East Pacific Rise the AMC presence and/or width does not appear to be related simply to small ridge-axis discontinuities.

Detailed seismic measurements are necessary in order to test hypotheses concerning AMC depth and its association with the seafloor bathymetry. Past seismic studies of along-axis variations in AMC depth have limitations in that they relied almost exclusively on two-way travel time to the reflection, and depth interpretations required assumptions about velocities above the AMC. Average velocities above the AMC are strongly influenced by the thickness of layer 2a because of its low velocity. In the absence of reliable layer 2a reflections the rapid increase in layer 2a thickness with age makes it critical that the ship position remains directly over the axis during reflection profiling. Initial studies of common midpoint (CMP) stacks from 9°N appeared to show AMC deepening, but in fact, the ship had wandered slightly off axis and was instead imaging the thickening of layer 2a [*Harding et al.*, 1993a]. With good layer 2a reflections, AMC depth variations can be estimated with some confidence from CMP data, provided the variations are large enough. However, for an accurate depth analysis, larger offsets, such as are provided by a wide-aperture profile (WAP), are required to capture refraction arrivals down to the lid of the AMC. Previous along-axis WAPs have lacked the necessary offset to provide accurate depth control to the AMC but have shown the feasibility of waveform inversion using this geometry [*Kappus et al.*, 1995]. Despite being a composite of one-dimensional measurements the WAP analysis described here is the most accurate determination to date of along-axis AMC depth variations.

Experiment and Site Description

The two-ship multichannel seismic experiment on the rise axis (TERA) was conducted in the spring of 1991 on the ultrafast spreading (150–162 mm/yr full rate [*Naar and Hey*, 1989; *DeMets et al.*, 1990]) portion of the East Pacific Rise between the 20.7°S propagating rift and the 13.5°S Garrett Fracture Zone [*Detrick et al.*, 1993a]. The experiment was designed to examine the seismic structure of the ridge crest using multichannel and ocean bottom seismograph techniques, with the objective of investigating crustal accretion processes and the nature of crustal magma bodies at the fast end of the spreading regime. Three institutions, Lamont-Doherty Earth Observatory (LDEO), Scripps Institution of Oceanography (SIO), and the University of Rhode Island, participated in the two-ship experiment using the R/V *Maurice Ewing* (LDEO) and the R/V *Thomas Washington* (SIO).

The work discussed here is an analysis of a 90-km wide-aperture profile (WAP) along the axis of the southern East Pacific Rise (SEPR) from 14°29.4′S to 13°39.5′S (line SEPR58-WAP1), just south of the Garrett Fracture Zone (Figure 1). A WAP is a two-ship profile: one ship has a streamer, both ships fire at staggered intervals, and the ships maintain a constant separation, thereby almost doubling the effective aperture of the profile [*Stoffa and Buhl*, 1979] (Figure 2). The R/V *Maurice Ewing* towed a 160-channel, 4 km streamer and fired its guns every 40 s, creating a 0.2–4.2 km shot gather every 40 s. The R/V *Thomas Washington* maintained a fixed distance of 7.4 km (4 nautical miles) behind the *Ewing* using radar and fired its guns every 40 s, staggered by 20 s from the *Ewing* shots, creating a 3.4–7.4 km range profile every 40 s. The *Washington* used a six-gun array with chamber sizes of 760, 640, 550, 300, 200 and 150 cubic inches for a total capacity of 2600 cubic inches (42.6 L). The *Ewing* gun array was designed to match the *Washington* array as closely as possible and used six guns with chamber sizes of 850, 540, 500, 350, 235, and 145 cubic inches for a total of 2620 cubic inches (42.9 L).

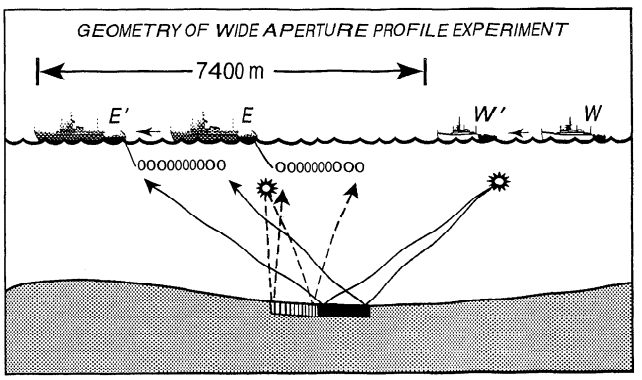

Figure 2. Geometry of wide-aperture profile (WAP) experiment. Ship E represents the R/V *Maurice Ewing*, and ship W represents the R/V *Thomas Washington*. The ships fire at staggered intervals and maintain a constant separation, thereby almost doubling the profile offset. As E moves to E′, W moves to W′, and the data from the shots at the two positions are combined to create a 7.4 km wide profile. (After *Kappus et al.* [1995]).

The rise axis along line SEPR58-WAP1 is remarkably flat and is associated with an increase in MgO content with respect to the area immediately south of the line [*Sinton et al.*, 1991], implying a more robust magma supply [*Langmuir et al.*, 1986]. However, superimposed on the increase with respect to the south, there is a decrease in MgO going north from 14°30′ toward the Garrett Fracture Zone through the area of the seismic line discussed here. Detailed analyses of CMP reflection profiles in the 14°15′S area of the SEPR have shown a relatively constant depth AMC with a width less than 1 km and a thin (200–250 m) layer 2a on axis, which thickens quickly with age to 500–600 m [*Kent et al.*, 1994]. Calculation of the cross-sectional area of 14°S, and other sections of the EPR, is discussed by *Scheirer and Macdonald* [1993], who suggest that the cross-sectional area is correlated with the magmatic budget of the spreading center.

Analysis Methods

To get an initial picture of along-axis structure, the *Ewing* data from 0.2–4.2 km range were processed as a common midpoint (CMP) profile. The nominal midpoint spacing of the data is 12.5 m, but gathering using this bin size yielded low-fold gathers due to the long shot interval and produced shingling in the stacked sections due to aliasing. The data were instead gathered using 100 m bins, increasing the reflection point smear but substantially improving the clarity of the stacks. Constant velocity stacks were employed to determine the stacking velocities of the features of interest: the top of the crust, layer 2a, and the top of the AMC. Stacking velocities of 1750 and 2200 m/s were chosen for the layer 2a and AMC reflections, respectively. Examination of the resulting stacked section (Figure 3) provided a starting point for the subsequent detailed velocity-depth analysis. It is clear from the stacked section that there is a gradual increase in travel time, from

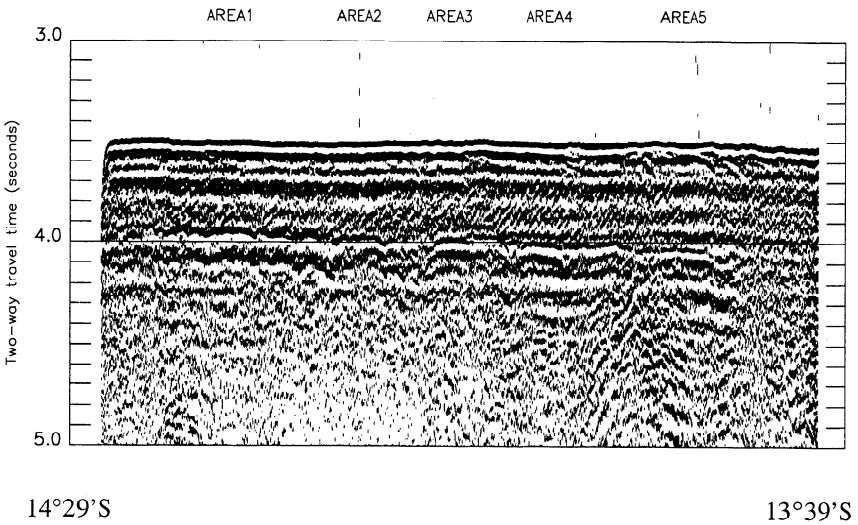

Figure 3. Stacked section of line SEPR58-WAP1. Areas analyzed in detail are marked. The AMC reflector can be seen getting progressively later in two-way travel time from slightly less than 4 s to slightly more than 4 s from the left to the right, respectively.

about 3.9 s to 4.0 s, to the AMC reflector from south to north. How this increase translates into depth is dependent on the velocity structure of the material overlying it. The stacked section allowed areas with a flat, bright AMC reflection to be picked out. One of the main objectives of the analysis was to do detailed WKBJ (i.e., one-dimensional) modeling of the upper crustal structure and depth to the AMC. It was desirable, therefore, to pick areas with a clear AMC reflection, and as close to a one-dimensional structure as possible.

Five areas of interest were selected, and the appropriate *Ewing* and *Washington* data were sorted into separate wide-aperature profile (WAP) gathers. The 100 m bin size yielded full, 160-fold gathers. To improve the signal to noise ratio, six consecutive full fold gathers were combined and stacked on a

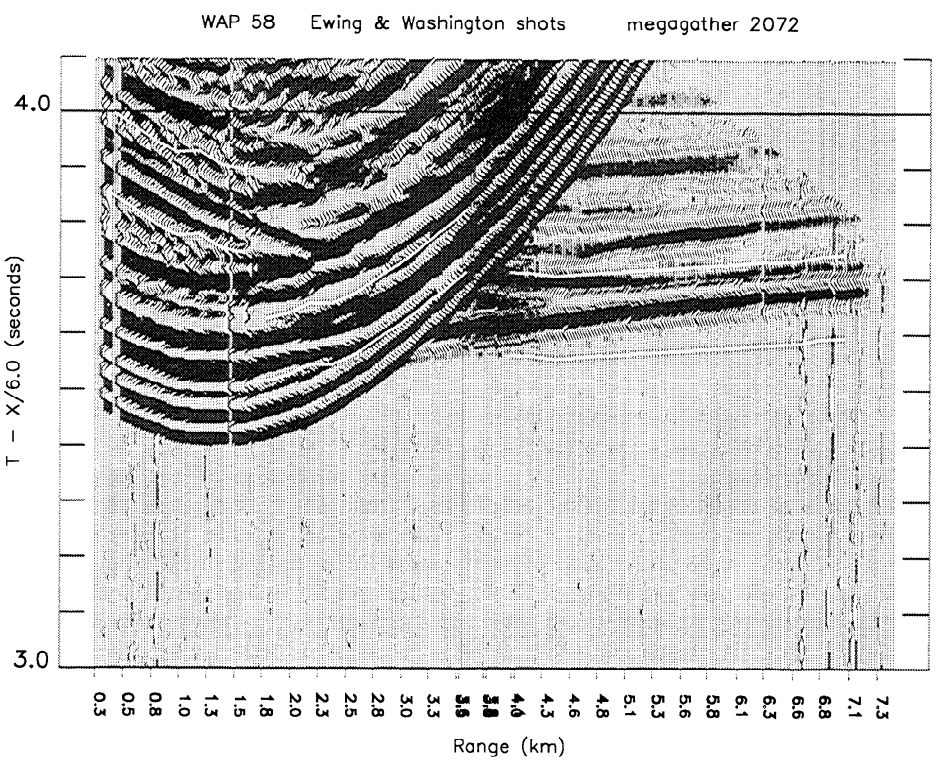

Figure 4. Record section showing megagather 2072, plotted with a reduction velocity of 6 km/s. The white lines mark the start and end points of the windows used in the genetic algorithm modeling. The window in the 0.3–1.6 km range contains AMC reflections. The 1.8–3.6 km window contains layer 2a arrivals. The 3.8–7.0 km window contains layer 2b refractions followed (in time) by the continuation of the AMC reflection. The area in the center of the plot with denser trace spacing is the overlap between the R/V *Thomas Washington* and R/V *Maurice Ewing* shots.

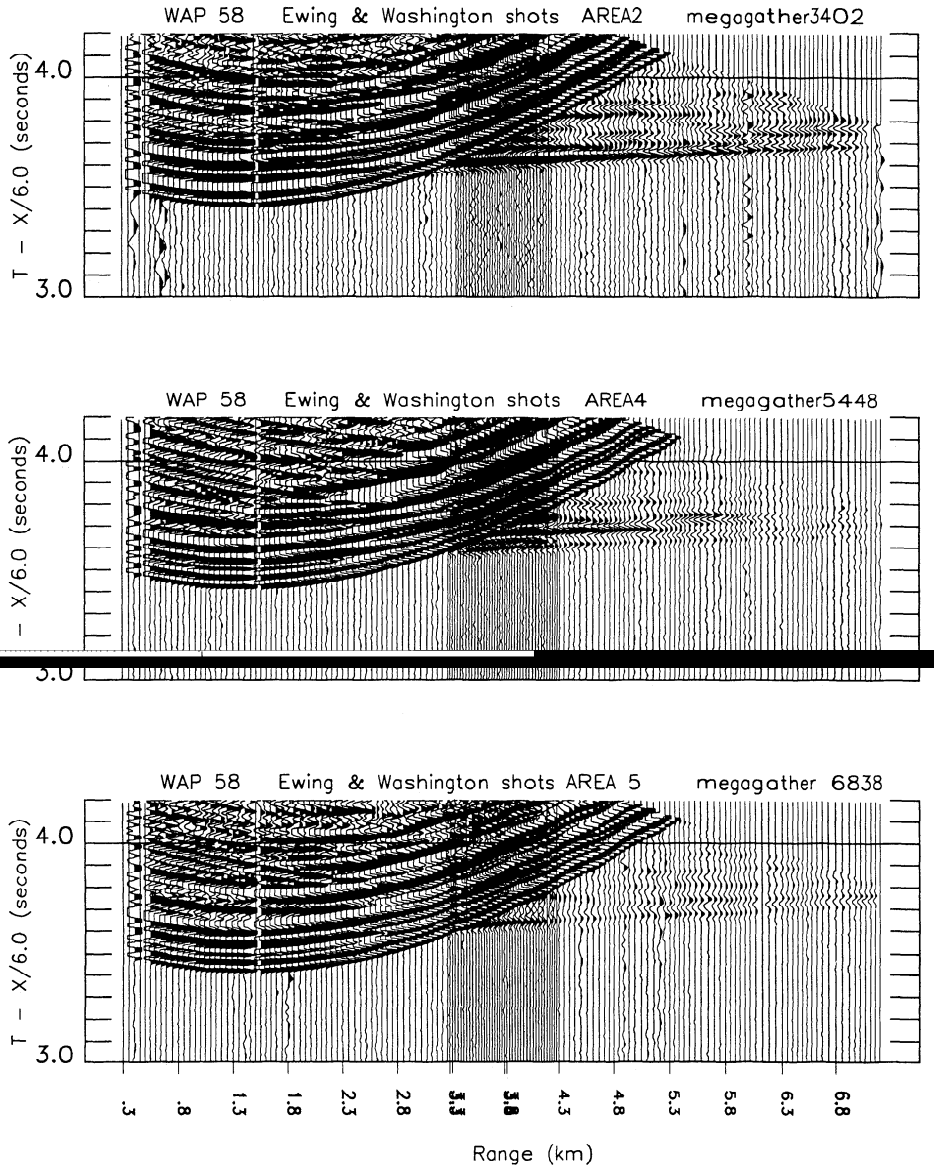

Figure 5. A selection of record sections from areas 2, 4, and 5 (from top to bottom), plotted with a reduction velocity of 6 km/s. The layer 2b refractions (~3.4–7.4 km) get progressively fainter as the north of the line is approached. For clarity, only every other trace is plotted. The area in the center of the plots with denser trace spacing is the overlap between the R/V *Thomas Washington* and R/V *Maurice Ewing* shots.

trace-by-trace basis to form one megagather with a 600 m bin size (Figure 4). Examples of megagathers from three of the areas are displayed in Figure 5. The refractions from layer 2b became weaker toward the north of the line and were severely disrupted in area 4 because the *Washington* wandered slightly off axis near this location.

In preparing the megagathers, the data were filtered using a 5–30 Hz Butterworth filter but were not subjected to predictive deconvolution as the bubble pulse was not considered strong enough to warrant such treatment. Noisy traces were removed from the megagathers, an event that occurred with increasing frequency toward the end of the line. The reason for the increase is unclear, though it was likely a degenerative problem with the streamer.

A genetic algorithm (GA) [e.g., *Goldberg*, 1989; *Sambridge and Drijkoningen*, 1992] was used to find velocity models that fit the data. A genetic algorithm mimics elements of the evolutionary process and aims, over successive generations, to produce better models, in our case models whose synthetic seismograms better fit the data. The GA works, producing a generation of models from the previous one, through the processes of selection, crossover, and mutation. The selection criteria favor better fitting models as parents for the next generation; crossover produces a pair of offspring from a pair of parent models; and mutation introduces an additional element of randomness at the "genetic" level, flipping randomly selected individual bits in the binary representation of the model. The GA provided a faster, more accurate, and more objective method of determining one-dimensional models than the trial-and-error model refining used in the past.

A set of initial velocity nodes and their allowable depth increment between nodes were input into the GA code used in this analysis [*Harding et al.*, 1993b; *Kappus and Harding*, 1993; A. J. Harding and M. E. Kappus, unpublished manuscript,

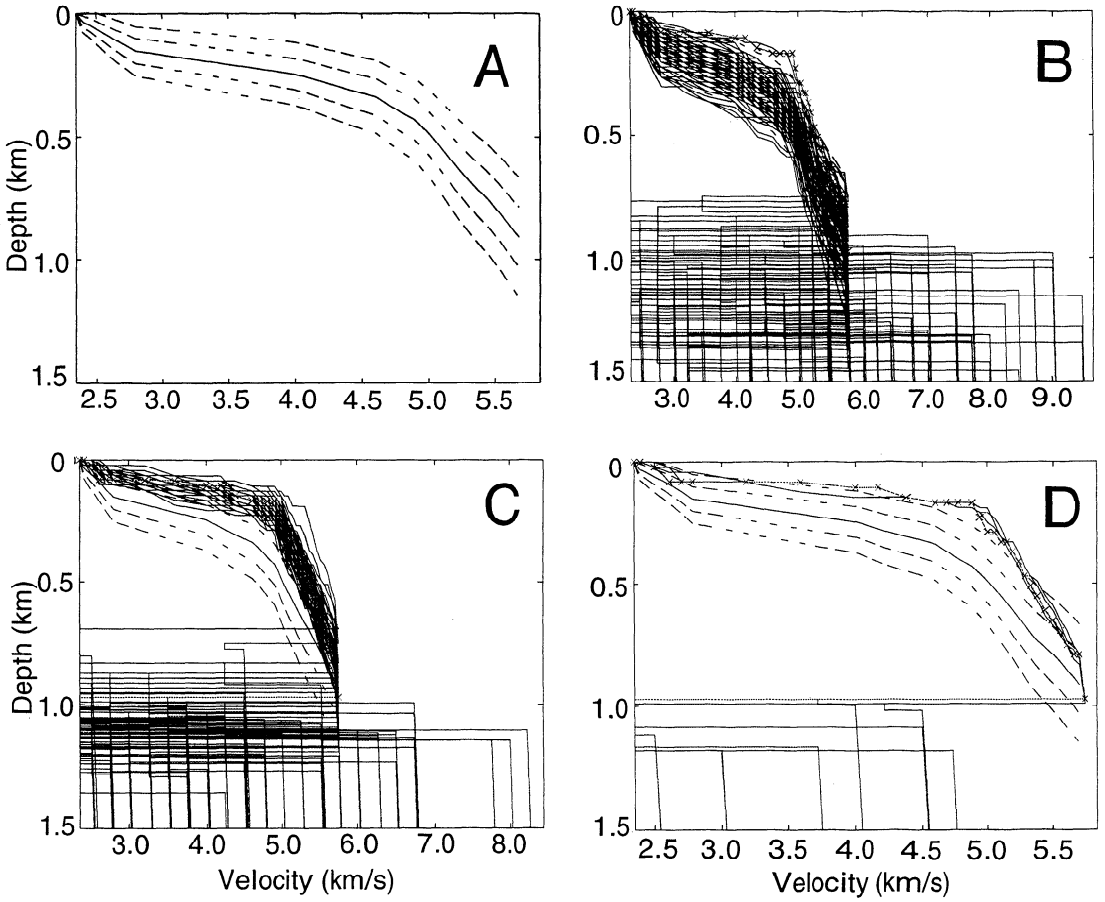

Figure 6. Progression of *P* wave velocity models using genetic algorithm. (a) The expected depth (solid) and 1 and 2 standard deviation bounds (dashed). The expected depth is made up of nodes chosen from a starting model which is determined through an inversion of WAP data from this line. (b) The 100 models making up the first generation. (c) The 100 models making up the last (fortieth) generation. (d) The top 10 models (by misfit) for all generations. Note that there is no control on the thickness of the AMC, since a reflection from the bottom of the AMC is not observed.

1996], and a starting generation of 100 models was created by a simple random walk that assigned depth increments between velocity nodes. For each model a misfit between WKBJ synthetic seismograms and the data was calculated for selected windows and used as the measure of relative fitness when choosing parent models for the next generation. The traces were allowed to be shifted slightly in time to optimize the fit in order to allow for slight shifts due to bathymetric effects. The overall misfit was taken as a (scalar) weighted combination of waveform misfit and time misfit [*Shaw*, 1988], with the weighting favoring a slight time shift when it improved the waveform misfit. The waveform misfit was taken as the root mean square of the individual trace differences, and the time misfit was taken as the root mean square of the shifts. Offspring models were created from parent models using single-point crossover and mutation. Although these processes are applied to the binary representation of the models, the incremental depth encoding ensures that they produce readily understood effects in the offspring. Crossover results in the swapping between parent models of velocity-depth curves below the crossover point, while mutation results in a small change in the depth increment between the affected velocity nodes. The affected nodes were selected randomly. For the work discussed here the crossover probability was set at 0.95, and the mutation probability was set at 0.01.

The GA was run for 40 generations of 100 models, by the end of which, hopefully, a successful model or series of models with a satisfactory misfit had been found. The misfit of the best models reached a plateau between 20 and 40 generations after which there was no significant improvement. Figure 6 shows an a example of the progression of the GA from the first generation to the last generation, and the final top 10 models. Since we are interested here in modeling the AMC reflection to determine the depth to the AMC, the basic GA code outlined above was augmented to produce models with a variable thickness, variable velocity magma lens. It was found to be critical that satisfactory models lay roughly within the velocity depth corridor formed by the initial generation of models in order for the GA code to succeed. Although the GA code proved to be relatively robust, it could not find satisfactory models when the layer 2a transition depth of the initial model was widely different from that of the data. A satisfactory transition depth was achieved by suitably balancing the allowable depth increments and number of velocity nodes. In this case a depth increment of 20 m and between 33 and 42 nodes were used.

The WKBJ seismograms could not reproduce all the features of the data so windows were picked from the megagathers to cover the areas of the AMC reflection, layer 2a reflection, and layer 2b refraction (Figure 4). The AMC and layer 2a reflections were picked from the *Ewing* shots, and the layer 2b

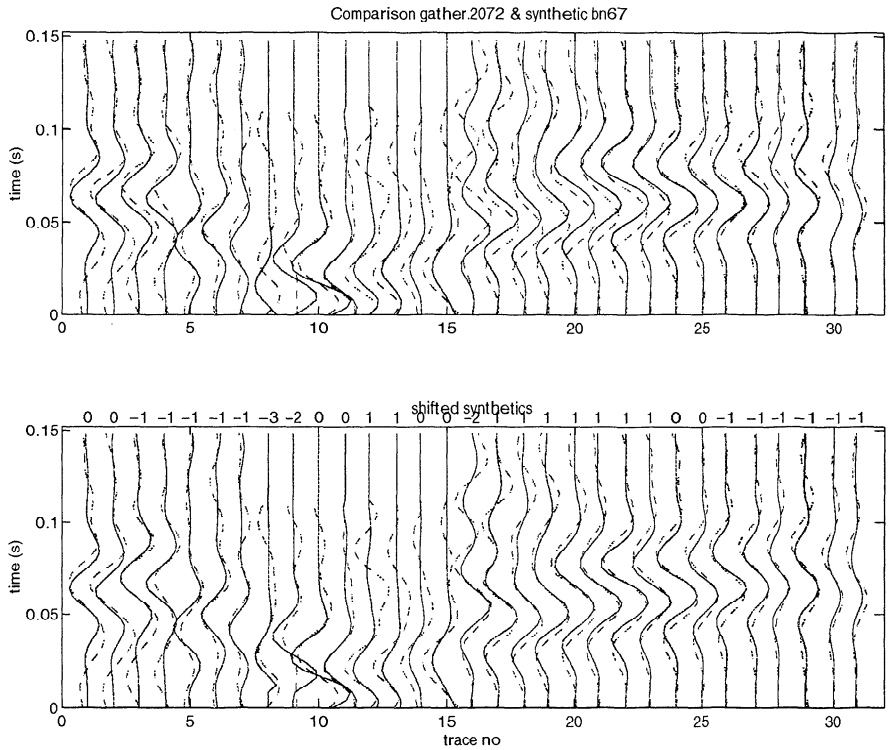

Figure 7. Fit of data windows (dashed) to synthetic windows (solid) for megagather 2072. The first seven traces window the AMC. The next eight traces window layer 2a arrivals. The last 16 traces window the layer 2b refraction. (top) The initial fit of the data to the synthetic. (bottom) The shifted fit. The synthetics are shifted to minimize the misfit. The amount of shifting required, which is shown at the top of each trace in number of sample intervals, is used to determine the time contribution to the overall misfit of the model. A shift of one or two sample intervals (4 ms) is not considered significant.

refraction was picked from the *Washington* shots. The overlap in data coverage lies between the ranges of 3.5 and 4.2 km, where the first emergence of layer 2b arrivals can be seen. Because the rest of the layer 2b arrival (4.2–7.4 km) is seen only in the *Washington* shots, it was prudent to use only *Washington* shots for the first couple of traces covering layer 2b to avoid problems associated with slight time shifts due to navigational inaccuracies and mismatches in source amplitude (the GA code attempts to match amplitude variations within a window, but the misfit does not penalize errors in the relative amplitude between windows). Only every eighth trace was used in the misfit calculations, resulting in a 200 m spacing between traces. Of the order of seven traces were picked for the AMC; eight were picked for the layer 2a, and up to 16 were picked for layer 2b. More traces were deemed unnecessary, since the misfit would be similar between close traces and more traces would only serve to increase the run time required. An example, from area 1, of the synthetic fit to the data for the specific windows is shown in Figure 7. The corresponding full seismogram fit is shown in Figure 8.

Results

Five areas were modeled in detail: area 1 was the farthest south and area 5 was the farthest north, closest to the Garrett Fracture Zone. These areas were picked based on the clarity of the AMC reflection observed in the constant velocity stacks. Two to three adjacent megagathers were modeled from each area as a check on the consistency of the local one-dimensional approximation. The results from area 4 are less reliable than those in the other areas because it was not clear that layer 2b was being matched correctly (Figure 9). Within each area the depth to the AMC for the different megagathers varies by no more than 20 m. The velocity depth models are shown in Figure 10, and the results are summarized in Table 1. The most notable observation from the results is that the AMC is getting progressively deeper toward the Garrett Fracture Zone (Figure 11).

Table 1. Depth to Top of Layer 2b and Depth to AMC Lid for the Gathers Analyzed From Areas 1–5

Area	Gather	Depth to Layer 2b, km	Depth to AMC, km	Distance From Start,[a] km
1	1976	0.187	0.99	23.021
1	2024	0.207	0.99	23.611
1	2072	0.167	0.97	24.139
2	3354	0.167	1.07	39.074
2	3402	0.147	1.07	39.634
2	3450	0.127	1.07	40.193
3	4328	0.187	1.09	50.422
3	4376	0.227	1.09	50.981
3	4424	0.207	1.11	51.54
4	5448	0.307	1.111	63.47
4	5496	0.247	1.131	64.029
5	6838	0.227	1.231	79.64
5	6886	0.207	1.211	80.223

[a]The distance of the gather from the southern end of the line (14°31.6′S to 112°37.4′W).

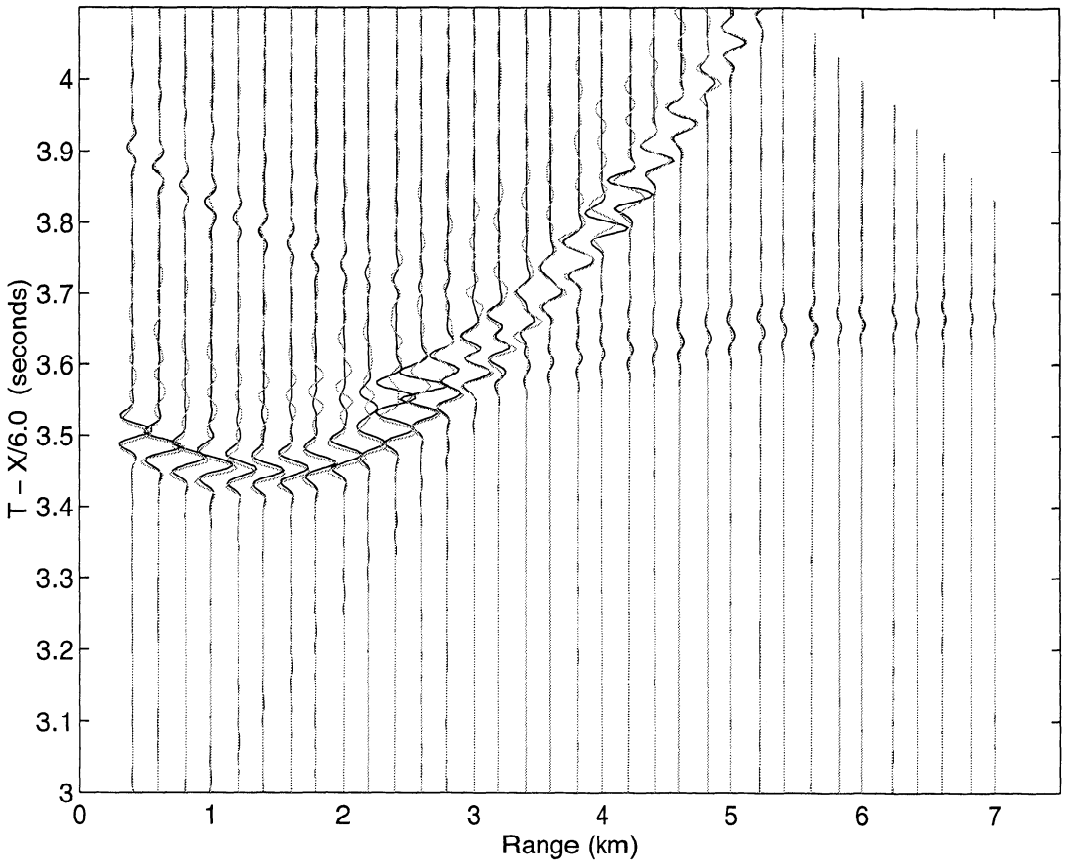

Figure 8. Overall fit of data windows (dotted) to synthetic windows (solid) for megagather 2072 plotted with a reduction velocity of 6 km/s. Note that even though the water wave arrival is well matched, only the windows shown in Figure 4 were actually used to calculate the misfit.

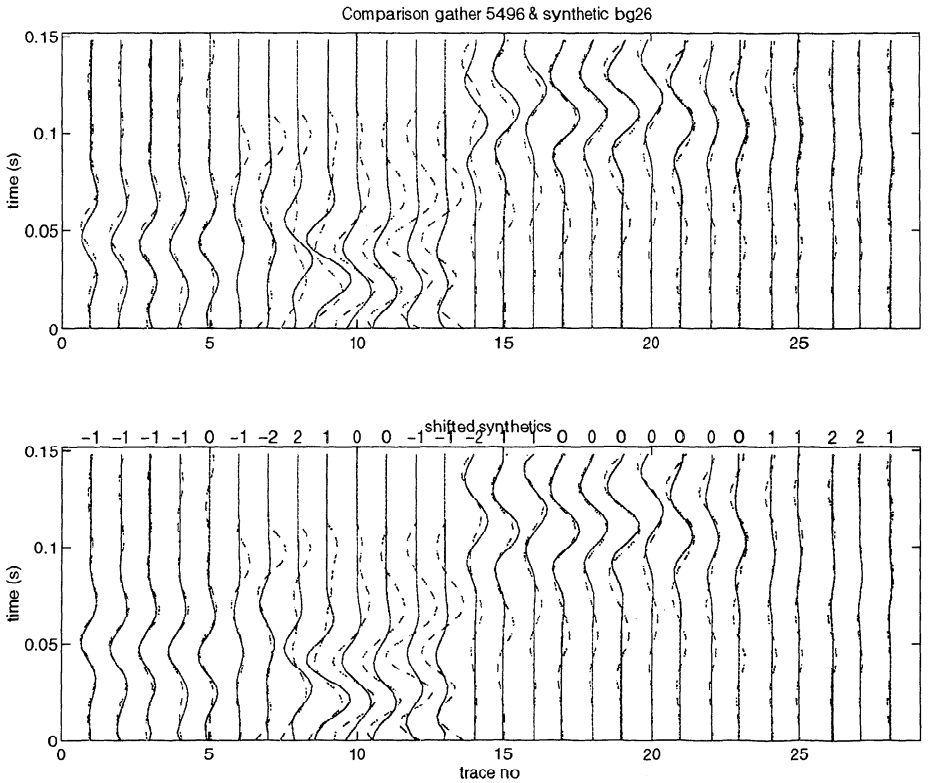

Figure 9. Fit of data windows (dashed) to synthetic windows (solid) for megagather 5496. (top) The initial fit of the data to the synthetic. (bottom) The shifted fit. Note that although there is a good fit to traces 1–5 (AMC) and a reasonable fit for traces 6–13 (layer 2a), the synthetics for traces 14–28 match the second arrival, which has a larger amplitude than the first.

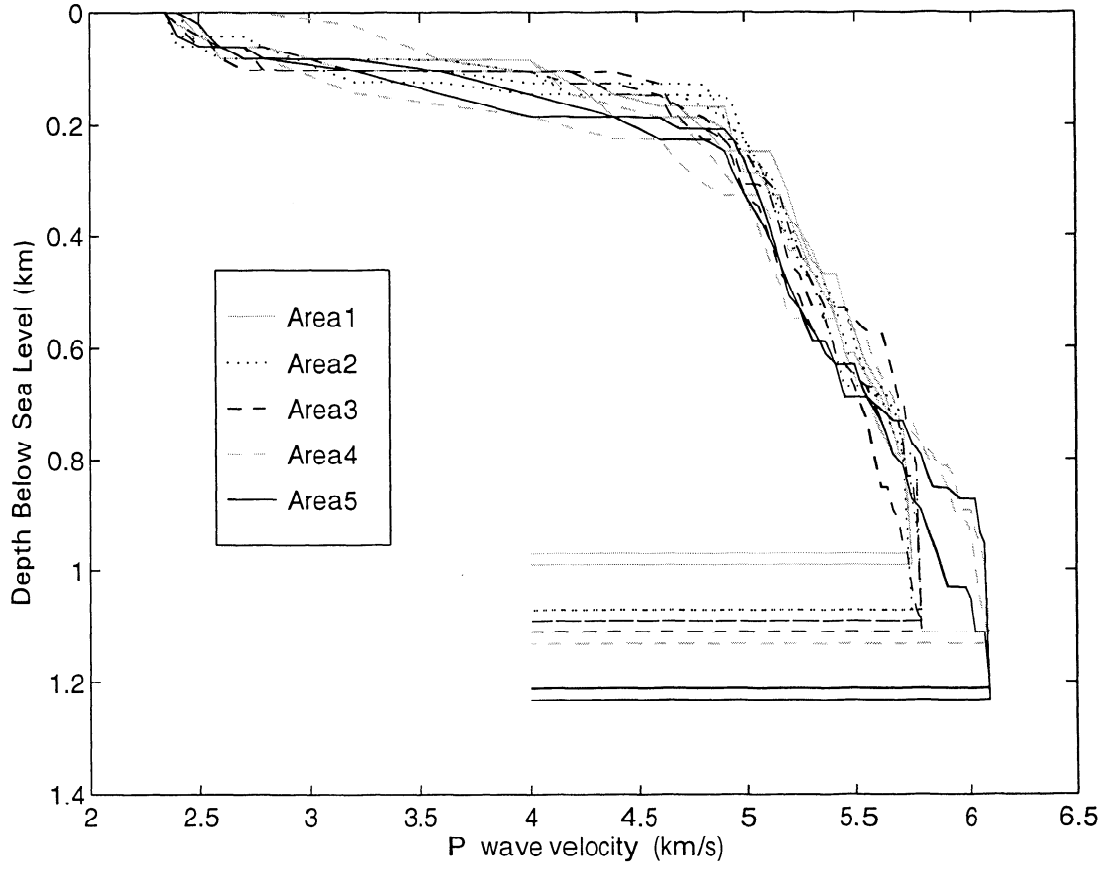

Figure 10. Velocity depth profiles for best fitting models of the megagathers in areas 1–5. Two or three profiles are shown for each area, since several adjacent gathers were modeled with each area (see Table 1). Note that the area 4 models are poorly constrained, particularly in the layer 2a/layer 2b transition region.

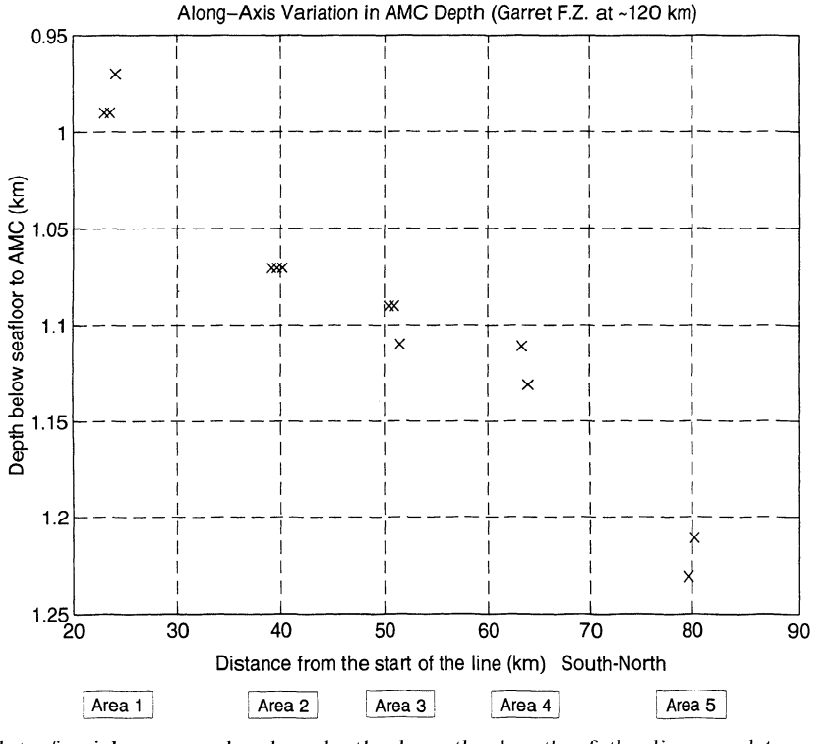

Figure 11. Plot of axial magma chamber depth along the length of the line, as determined from the one-dimensional velocity depth profiles. The Garrett Fracture Zone is located at about 120 km in this coordinate scheme.

The modeling became increasingly difficult toward the north, primarily because the initial layer 2b arrival became faint. The situation was aggravated by the fact that noise on the traces and the number of bad traces also increased toward the north. It may be that the structure was such that more scattering occurred farther north and hence less coherent energy was returned. An initial plausible explanation for the faint layer 2b arrival is that the velocity gradient in layer 2b was lower to the north. However, this explanation is not upheld by the models: the velocity directly above the AMC increases as the AMC deepens, making low gradients less likely. Note that the relative consistency of the AMC depth within the different areas increases confidence in the results even where the modeling was more difficult.

The difficulty in modeling area 4 data stemmed from the fact that the megagathers in this area recorded a pair of layer 2b arrivals (Figure 5) and that the GA preferentially fitted the secondary arrival. Modeling did, however, obtain excellent fits to layer 2a and the AMC and gave very consistent AMC depth results for a variety of different windowing and weighting schemes. The most likely explanation for the dual layer 2b refractions is that the propagation paths are not one-dimensional in this area because the *Washington* wandered very slightly off axis near this location (Figure 1).

Apart from the area 4 results, which were poorly constrained (as discussed above), there does not appear to be a substantial variation in the thickness of layer 2a along axis. The velocity increases rapidly from 2.35 to about 4.9 km/s within the top 200 m. After that there is a low gradient corresponding to layer 2b. All the areas have a layer 2a thickness of around 180 m ± 60 m, which matches closely the estimated layer 2a thickness of 200–250 m observed by *Kent et al.* [1994] on cross-axis CMP profiles across the southern half of the line. Area 5 does have a slightly thicker layer 2a than the other areas (about 220 m ± 20 m). The thicker layer 2a for area 5 in no way invalidates the observation of a deeper magma chamber in this area. Layer 2a is of the order of 40 m thicker, whereas the AMC is about 260 m deeper. The problem with the deeper layer 2a leading to false depths of the AMC arises when layer 2a is not well constrained, and a relatively small change in thickness at its slow velocities can look like a big change in thickness at higher (layer 2b) velocities. In this experiment, layer 2a is well constrained. Areas 2 and 5 appear to have the most abrupt transition between layer 2a and layer 2b.

Discussion

Before any comparison is made between the results discussed here and results from previous seismic work, it should be reemphasized that the depth resolution of this study is considerably better than conventional CMP derived estimates and is comparable to that of expanding spreading profiles (ESPs) because the 7.4 km maximum range captures refraction arrivals down to the lid of the AMC. The advantage of WAPs is that they provide a whole series of one-dimensional models along a line, allowing accurate measurements of variations along the line. Previously along-axis AMC depth variations have been mapped using CMPs, or smaller offset WAPs, which did not image the full range of refracted layer 2b arrivals. In the past the primary method of observation was two-way travel time, which made depth estimates susceptible to unmapped variations in layer 2a or 2b thickness and velocity.

At fast spreading ridges the relative importance of primarily two-dimensional versus three-dimensional processes in mantle flow and crustal accretion is still unclear. At slow spreading ridges such as the Mid-Atlantic Ridge, mantle upwelling and crustal accretion are both thought to be primarily three-dimensional at the segment scale, with focused upwelling of magma within the mantle leading to characteristically thicker crust at the center of a segment and thinner crust at the ends [*Lin et al.*, 1990; *Tolstoy et al.*, 1993]. The absence of steady state magma chambers at slow spreading ridges precludes the possibility of magma redistribution within the crust, but their presence at fast spreading ridges means that the relative uniformity of crustal thickness may be ascribed to a transition to two-dimensional upwelling within the mantle, to the effective smoothing of focused upwelling by along-axis flow [*Macdonald et al.*, 1988], or to some combination of the two. Detailed along-axis mapping of axial magma chamber and upper crustal structure represents a necessary step in trying to distinguish between these possibilities. In this study we have demonstrated the possibility of obtaining accurate and quasi-continuous depth estimates for the AMC from along-axis WAPs. The principal result of the study is the discovery of the deepening of the AMC by ~240 m over 60 km as it approaches the Garrett Fracture Zone.

The systematic deepening of the AMC contrasts with morphological measures such as axial depth and cross-sectional area which show no systematic variation over the same interval [*Scheirer and Macdonald*, 1993]. Seismic reflection data from 17°S have been interpreted as supporting the notion of a direct correlation between axial morphology and ridge magmatic state [*Mutter et al.*, 1995]. However, recent detailed comparisons of AMC properties along the East Pacific Rise [*Hussenoeder et al.*, 1996] indicate that axial morphology is not simply related to AMC thickness, depth, or velocity.

Systematic trends in axial depth and cross-sectional area have been proposed as indicators of focused upwelling and along-axis flow [*Macdonald et al.*, 1988; *Scheirer and Macdonald*, 1993], and their absence here can be taken as evidence against a single central magma injection point for the 14°S segment. However, one should make a distinction between the possibility of along-axis flow within the melt lens and flow that extends beneath the lens. If along-axis flow is concentrated primarily within the relatively low-velocity, high-melt fraction lens, it may not have an observable bathymetric effect. In addition, the direction of flow within the lens conduit is uncertain; gravitationally driven flow within the lens conduit could be toward rather than away from the center of the segment if, as has been proposed [*Hooft and Detrick*, 1993], the magma is positively buoyant. Conversely, centralized upwelling and/or volatile exsolution could create a pressure gradient within the conduit that would reverse the flow direction. The principal difficulty with proposing segment scale flow within the lens conduit is the presence of distinct geochemical signatures such as the one at 14°27′S [*Sinton et al.*, 1991] which indicates the existence of some form of mixing boundary [*Kent et al.*, 1994].

One factor that must be considered, is the influence of the Garrett transform on the magma chamber depth and mantle upwelling patterns. MgO content indicates a decrease in the degree of melting from 14°30′S north toward the Garrett (13°24′S) [*Sinton et al.*, 1991], although the trend is not as clear within the latitudes of the areas studied here (~14°24′S to 13°48′S). At slow spreading ridges, there is ample evidence from both theoretical models [*Parmentier and Phipps-Morgan*,

1990] and geophysical measurements [*Tolstoy et al.*, 1993; *Detrick et al.*, 1993b] that even small offsets are associated with reduced mantle upwelling and thinner crust. The geophysical signals are expected to be muted at fast spreading ridges because of the increased rates of upwelling and the lower mantle viscosities. We propose that the measured increase in magma chamber depth is one such signal, indicating a systematic reduction in mantle upwelling toward the Garrett transform. In this view, mantle upwelling and crustal accretion are predominantly two-dimensional processes that do not require significant along-axis flow; the principal effect of the reduced upwelling is to increase the equilibrium depth of the magma lens that balances magma heat supply with the hydrothermal and conductive cooling. It should be emphasized that this model refers only to the long wavelength trend being measured by the WAP results. The current data are certainly not sufficient to distinguish between a basically sheet-like magma supply to the crust and multiple closely spaced local injection centers. Along-axis variations in the width of the AMC [*Kent et al.*, 1993a, b, 1994] and three-dimensional pinching of the axial low-velocity volume [*Toomey et al.*, 1990] imply that within the crust, accretion is three-dimensional on length scales of the order of 10 km, at least to some degree. The along-axis reflection profile for 14°S shows variations on this scale, although at least some of these variations are probably attributable to upper crustal variations and ship wander relative to the rise axis.

If a systematic reduction in mantle upwelling is responsible for the observed deepening of the AMC, then it appears that morphological variations are not good indicators of magma supply, at least at the fine scales observed here. However, the AMC deepening could also be a temporal phenomenon. Further analyses of off-axis crustal thickness data, collected as part of the TERA experiment, may help answer this question by determining crustal thickness and relative layer 2/layer 3 thicknesses in this area.

Conclusions

In conclusion, the AMC deepens consistently by a total of 260 m over a distance of about 60 km. This is interpreted as systematic reduction of mantle upwelling due to the proximity to the Garrett Fracture Zone, which is the first major interruption of hundreds of kilometers of continuous ridge axis. There is no clear correlation between the AMC deepening and axial depth or cross-sectional area, which is inconsistent with models that propose that these properties should be related. The AMC along this 14°S portion of the EPR is approximately 400–600 m shallower than the AMC observed at 9°N and supports the hypothesis that AMC depth directly correlates with spreading rate [*Purdy et al.*, 1992; *Phipps Morgan and Chen*, 1993].

Layer 2a is observed to remain fairly constant in thickness of the order of 180 m ± 60 m. This thickness is not significantly different than that observed at 13°N [*Kappus et al.*, 1995]. The on-axis thickness of layer 2a does not therefore appear to have a dependence on spreading rate, at least within the fast end of the spectrum, thus supporting *Kappus et al.*'s [1995] hypothesis that layer 2a thickness is controlled by the dynamics of emplacement rather than the level of the magma supply.

This experiment has shown that using WAPs and accurate modeling techniques, it is possible to map AMC depth with previously unachieved accuracy. More of these types of measurements in others areas will help answer the question of the two-dimensional versus three-dimensional nature of crustal formation at fast spreading ridges.

Acknowledgments. We would like to thank Mary Kappus for the use of her genetic algorithm code and Paul Henkart and the Scripps Industrial Associates for the use of the SIOSEIS processing package. We thank Paul Earle for helpful discussions and Figure 2. We thank two anonymous reviewers and Y. John Chen for constructive reviews. We also thank the captains and crews of the R/V *Thomas Washington* and R/V *Maurice Ewing*. This work was carried out under grants OCE90-12596 and OCE94-01864.

References

Caress, D. W., M. S. Burnett, and J. A. Orcutt, Tomographic image of the axial low velocity zone at 12°50′N on the East Pacific Rise, *J. Geophys. Res.*, *97*, 9243–9264, 1992.

Christeson, G. L., G. M. Purdy, and J. G. Fryer, Structure of young crust at the East Pacific Rise, *Geophys. Res. Lett.*, *19*, 1045–1048, 1992.

Christeson, G. L., G. M. Purdy, and J. G. Fryer, Seismic constraints on the shallow crustal emplacement processes at the fast spreading East Pacific Rise, *J. Geophys. Res.*, *99*, 17,957–17,953, 1994.

DeMets, C., R. G. Gordon, D. F. Argus, and S. Stein, Current plate motions, *Geophys. J. Int.*, *101*, 425–478, 1990.

Detrick, R. S., P. Buhl, E. Vera, J. Mutter, J. Orcutt, J. Madsen, and T. Brocher, Seismic structure of the southern East Pacific Rise, *Science*, *259*, 35–42, 1993a.

Detrick, R. S., R. S. White, G. M. Purdy, Crustal structure of North Atlantic fracture zones, *Rev. Geophys.*, *31*, 439–458, 1993b.

Goldberg, D. E., *Genetic Algorithms in Search, Optimization, and Machine Learning*, Addison-Wesley, Reading, Mass., 1989.

Harding, A. J., J. A. Orcutt, M. E. Kappus, E. E. Vera, R. S. Detrick, and T. M. Brocher, Structure of young oceanic crust at 13°N on the East Pacific Rise from expanding spread profiles, *J. Geophys. Res.*, *94*, 12,163–12,196, 1989.

Harding, A. J., G. M. Kent, and J. A. Orcutt, A multichannel seismic investigation of upper crustal structure at 9°N on the East Pacific Rise: Implications for crustal accretion, *J. Geophys. Res.*, *98*, 13,925–13,944, 1993a.

Harding, A. J., J. A. Orcutt, M. E. Kappus, R. S. Detrick, G. M. Kent, J. C. Mutter, and P. Buhl, Inversion of expanding spread profile data from 17°S on the East Pacific Rise using a genetic algorithm (abstract), *Eos Trans. AGU*, *74*(43), Fall Meet. Suppl. 604, 1993b.

Hooft, E. E., and R. S. Detrick, The role of density in the accumulation of basaltic melt at mid-ocean ridges, *Geophys. Res. Lett.*, *20*, 423–426, 1993.

Hussenoeder, S. A., J. A. Collins, G. M. Kent, and R. S. Detrick, Seismic analysis of the axial magma chamber reflector along the southern East Pacific Rise from conventional reflections profiling, *J. Geophys. Res.*, *101*, 22,087–22,105, 1996.

Kappus, M. E., and A. J. Harding, Using genetic algorithms to produce seismic velocity models for synthetic reflection/refraction data (abstract), *Eos Trans. AGU*, *74*(43), Fall Meet. Suppl. 393–394, 1993.

Kappus, M. E., A. J. Harding, and J. A. Orcutt, A baseline for upper crustal velocity variations along the East Pacific Rise at 13°N, *J. Geophys. Res.*, *100*, 6143–6161, 1995.

Kent, G. M., A. J. Harding, and J. A. Orcutt, Distribution of magma beneath the East Pacific Rise between the Clipperton Transform and the 9°17′N deval from forward modeling of common depth point data, *J. Geophys. Res.*, *98*, 13,945–13,970, 1993a.

Kent, G. M., A. J. Harding, and J. A. Orcutt, Distribution of magma beneath the East Pacific Rise near the 9°03′N overlapping spreading center from forward modeling of common depth point data, *J. Geophys. Res.*, *98*, 13,971–13,995, 1993b.

Kent, G. M., A. J. Harding, J. A. Orcutt, R. S. Detrick, J. C. Mutter, and P. Buhl, Uniform accretion of oceanic crust south of the Garrett transform at 14°15′S on the East Pacific Rise, *J. Geophys. Res.*, *99*, 9097–9116, 1994.

Langmuir, C. H., J. F. Bender, and R. Batiza, Petrological and tectonic segmentation of the East Pacific Rise, *Nature*, *322*, 422–429, 1986.

Lin, J., G. M. Purdy, H. Schouten, J.-C. Sempere, and C. Zervas, Evidence from gravity data for focused magmatic accretion along the Mid-Atlantic Ridge, *Nature*, *344*, 627–632, 1990.

Macdonald, K. C., P. J. Fox, L. J. Perram, M. F. Eisen, R. M. Haymon,

S. P. Miller, S. M. Carbotte, M.-H. Cormier, and A. N. Shor, A new view of the mid-ocean ridge from the behaviour of ridge-axis discontinuities, *Nature*, *335*, 217–225, 1988.

McClain, J. S., J. A. Orcutt, and M. Burnett, The East Pacific Rise in cross section: A seismic model, *J. Geophys. Res.*, *90*, 8627–8639, 1985.

Mutter, J. C., S. M. Carbotte, W. Su, L. Xu, P. Buhl, R. S. Detrick, G. M. Kent, J. A. Orcutt, and A. J. Harding, Seismic images of active magma systems beneath the East Pacific Rise 17°05′ to 17°35′S, *Science*, *268*, 391–395, 1995.

Naar, D. F., and R. N. Hey, Speed limit for oceanic transform faults, *Geology*, *17*, 420–422, 1989.

Parmentier, E. M., and J. Phipps Morgan, Spreading rate dependence of three-dimensional structure in oceanic spreading centres, *Nature*, *348*, 325–328, 1990.

Phipps Morgan, J., and Y. J. Chen, Dependence of ridge-axis morphology and geochemistry on magma supply and spreading rate, *Nature*, *364*, 706–708, 1993.

Purdy, G. M., New observations of the shallow seismic structure of young oceanic crust, *J. Geophys. Res.*, *92*, 9351–9362, 1987.

Purdy, G. M., and R. S. Detrick, Crustal structure of the Mid-Atlantic Ridge at 23°N from seismic refraction studies, *J. Geophys. Res.*, *91*, 3739–3762, 1986.

Purdy, G. M., L. S. L. Kong, G. L. Christeson, and S. C. Solomon, Relationship between spreading rate and the seismic structure of mid-ocean ridges, *Nature*, *355*, 815–817, 1992.

Sambridge, M., and G. Drijkoningen, Genetic algorithms in seismic waveform inversion, *Geophys. J. Int.*, *109*, 323–342, 1992.

Scheirer, D. S., and K. C. Macdonald, Variation in cross-sectional area of the axial ridge along the East Pacific Rise: Evidence for the magmatic budget of a fast spreading center, *J. Geophys. Res.*, *98*, 7871–7886, 1993.

Shaw, P. R., Waveform inversion of time-corrected seismic refraction data, *Geophys. J.*, *93*, 75–90, 1988.

Sinton, J. M., S. M. Smaglik, J. J. Mahoney, and K. C. Macdonald, Magmatic processes at superfast spreading mid-ocean ridges: Glass compositional variations along the East Pacific Rise 13°–23′S, *J. Geophys. Res.*, *96*, 6133–6155, 1991.

Stoffa, P. L., and P. Buhl, Two-ship multichannel seismic experiments for deep crustal studies: Expanded spread and constant offset profiles, *J. Geophys. Res.*, *84*, 7645–7660, 1979.

Tolstoy, M., A. J. Harding, and J. A. Orcutt, Crustal thickness on the Mid-Atlantic Ridge: Bull's eye gravity anomalies and focused accretion, *Science*, *262*, 726–729, 1993.

Toomey, D. R., G. M. Purdy, S. C. Solomon, and W. S. D. Wilcock, The three-dimensional seismic velocity structure of the East Pacific Rise near latitude 9°30′N, *Nature*, *347*, 639–645, 1990.

Vera, E. E., J. C. Mutter, P. Buhl, J. A. Orcutt, A. J. Harding, M. E. Kappus, R. S. Detrick, and T. Brocher, The structure of 0 to 0.2 Ma old oceanic crust at 9°N on the East Pacific Rise from expanded spread profiles, *J. Geophys. Res.*, *95*, 15,529–15,556, 1990.

P. Buhl, J. C. Mutter, and M. Tolstoy, Lamont-Doherty Earth Observatory, 103 Geoscience, Route 9W, Palisades, NY 10964. (e-mail: buhl@ldeo.columbia.edu; jcm@ldeo.columbia.edu; tolstoy@ldeo.columbia.edu)

R. S. Detrick and G. M. Kent, Department of Geology and Geophysics, Woods Hole Oceanographic Institution, Woods Hole, MA 02543. (e-mail: bobd@copper.whoi.edu)

A. J. Harding, and J. A. Orcutt, Institute of Geophysics and Planetary Physics, Scripps Institution of Oceanography, La Jolla, CA 92093-0225. (e-mail: jorcutt@igpp.ucsd.edu)

(Received January 29, 1996; revised October 10, 1996;
accepted October 15, 1996.)